THE AMERICAN SOCIETY OF MECHANICAL ENGINEERS
345 E. 47 St., New York, N.Y. 10017

86-GT-235

Viscous/Inviscid Computations of Transonic Separated Flows Over Solid and Porous Cascades

CHARLES R. OLLING and GEORGE S. DULIKRAVICH
Postdoctoral Fellow Assistant Professor
Department of Aerospace Engineering and
Engineering Mechanics
University of Texas at Austin, Austin TX 78712

ABSTRACT

A complete viscous-inviscid interaction is performed that reliably computes steady two-dimensional, subsonic and transonic attached and separated flows for cascades of airfoils. A full-potential code was coupled with both a laminar/transition/ turbulent integral boundary-layer/turbulent wake code and the finite-difference boundary-layer code using the semi-inverse methods of Carter and Wigton. The transpiration coupling concept was applied with an option for a porous airfoil with passive and active physical transpiration. Examples are presented which demonstrate that such flows can be calculated with engineering accuracy by these methods. Carter's update formula gives smoother solutions for a strong shock that Wigton's update formulas, although Wigton's formulas are preferred in the early coupling cycles. The computations show that passive physical transpiration can lead to a lower drag coefficient and higher lift coefficient, a weaker shock and elimination of shock-induced separation. The extent of the porous region and permeability factor distribution of the porous region must be chosen carefully if these improvements are to be achieved.

INTRODUCTION

Background

Any meaningful computation of separated transonic two-dimensional flows for cascades requires the inclusion of viscous boundary layer and wake effects. Reviews of procedures for calculating viscous-inviscid interaction in transonic flow about isolated airfoils have been presented by Olling [1], Lock [2], Lock and Firmin [3], Melnik [4], LeBalleur [5], Jameson [6] and Cebeci, Stewartson and Whitelaw [7].

The boundary layer can be calculated in the direct or inverse mode. In the direct mode the velocity or pressure on the matching surface between the viscous and inviscid part of the flow field is specified. In the inverse mode some other quantity (the forcing function) is specified, such as the displacement thickness (δ^*), mass flux defect (Q) or skin friction coefficient (C_f). Present finite-difference and integral methods in general must be operated in the inverse mode to calculate extended separated regions in practical computations, when steady-state first-order boundary layer theory is used (see Drela and Thompkins [8] for an exception for a finite-difference method). An alternative way to simulate massive separation is to compute the detached streamline where the boundary layer separates from the airfoil and then use this streamline as part of the effective airfoil surface (Hirsch and Janssens [9] and Dvorak and Choi [10].

The matching between the inviscid and viscous calculations can occur on any of three different surfaces: the surface of the airfoil and the wake centerline, the displacement surface or the edge of the boundary layer and wake δ (Murman and Bussing [11]). In the first case an equivalent transpiration boundary condition is used in the inviscid calculation. This case will be called the transpiration coupling concept. It obviates the necessity of regenerating the inviscid grid after each coupling cycle and represents the best existing method [1]. Several types of strong interaction methods have been devised. The simplest approach, called the semi-inverse method, computes part or all of the boundary layer and wake in the inverse mode. An initial guess for the forcing function must be made. The resulting viscous boundary-layer edge velocity or pressure is compared with the inviscid velocity or pressure on the matching surface. If these differ then the forcing function and the coupling boundary conditions are updated. Several methods have been proposed for updating the forcing function during the viscous-inviscid iterations by Carter [12], LeBalleur [13], Wigton [14] and Gordon and Rom [15]. This type of strong interaction has been favored by many investigators because it allows one to make the minimum amount of changes to the inviscid code, which is usually more complex than the viscous code.

It should be noted that first-order boundary-layer theory neglects the normal-pressure gradient effect due to the curvature of streamlines inside the boundary layer and wake. In the near-wake region this effect leads to a jump in the tangential velocity component along the wake centerline in the inviscid code. It

Presented at the International Gas Turbine Conference and Exhibit
Dusseldorf, West Germany—June 8-12, 1986

will be called the wake curvature effect and two approximate theories have been proposed to correct for it (Melnik [4] and Lock and Firmin [3]).

POROUS AIRFOILS

Shock-free or nearly shock-free transonic airfoils and cascades have favorable properties, such as minimum wave drag and no or reduced shock-induced separation. To design such airfoils, one approach has been to modify the airfoil shape (Dulikravich and Sobieczky [16]). Another method of achieving shock self-cancellations is to modify the surface boundary conditions on the airfoil, such as by allowing for physical transpiration by making the airfoil surface porous (Savu and Trifu [17], Savu, Trifu and Dumitrescu [18], Krogmann, Stanewsky and Thiede [19,20], Nagamatsu, Dyer and Ficarra [21]), Ram, Vemuru and Harvey [22], Chen, Chow, Holst and Van Dalsem [23], and Olling [1]). The latter approach may be applied in an active (or forced) transpiration mode or in a passive transpiration mode. An example of a passive method is allowing the plenum (cavity) pressure (under the porous airfoil surface) to adjust to a value that is in equilibrium with Darcy's law for porous material and the external flow. In this case, the net mass flow through the perforated airfoil surface is zero.

The computer codes developed as a part of this [1] study can simulate the passive transpiration effects of a perforated airfoil surface with a cavity located underneath. Darcy's law is used to determine the physical transpiration velocity [17]

$$v_w = \sigma(p_p - p_w)$$

$$\sigma = \bar{\sigma}/(\rho_\infty q_\infty)$$

where p_w is the airfoil surface pressure, p_p is the plenum pressure (assumed to be constant), σ is the permeability factor, $\bar{\sigma}$ is the nondimensional permeability factor, and ρ_∞ and q_∞ are the upstream density and speed, respectively. A value of $\bar{\sigma} = 0.6$ corresponds to a geometrical porosity of about 10 percent [18]. The plenum pressure is computed from

$$p_p = \int_s \rho\bar{\sigma}p_s ds \Big/ \int_s \rho\bar{\sigma} ds$$

where s is the airfoil surface arc length.
The physical transpiration velocity normalized by the critical speed of sound is

$$\frac{v_w}{a^*} = \frac{\bar{\sigma}M_\infty^*}{\gamma M_\infty^2}\left[\frac{\int_s \bar{\sigma}\frac{\rho}{\rho^*}\frac{p_s}{p_\infty}\frac{ds}{c}}{\int_s \bar{\sigma}\frac{\rho}{\rho^*}\frac{ds}{c}} - \frac{p_s}{p_\infty}\right]$$

where the asterisk denotes a critical value.

Two distributions of $\bar{\sigma}$ can be specified in the input of the present version of the code [24]. These are a uniform distribution and a peaked distribution having a maximum inside the porous region and smooth tapering to zero at the ends of the region. The chordwise coordinates of the beginning (x_1) and end (x_2) of the porous region and the location of the maximum permeability (x_m) on the upper and lower sides of the airfoil are inputted.

INTEGRAL BOUNDARY-LAYER CODE

Laminar Boundary Layer

The boundary layer is assumed to be divided into laminar, transitional and fully turbulent regions in the streamwise direction. Near the leading edge of the airfoil the boundary layer is assumed to be laminar. The attached laminar boundary layer is computed in the direct mode by a modified form of a compressible Thwaites method (Rott and Crabtree [25]; see Appendix A for details). The tangential inviscid velocity on the airfoil surface u_i is specified. If laminar separation is indicated, the boundary layer is in the present code assumed to transition abruptly to fully turbulent flow.

Transition Region

Two options are available for determining transition. One option is to enforce abrupt transition at a specified point (no transition region). The other option is to calculate the transition region from the empirical method of Abu-Ghannam and Shaw [26] modified for compressibility. The start of transition is determined from an empirical correlation for the incompressible momentum thickness Reynolds number as a function of the free-stream turbulence level and an incompressible streamwise velocity gradient parameter. Other correlations are used to determine the extent of the transition region and the momentum thickness at the end of transition. Additional correlations then allow the momentum thickness, shape factor and skin friction coefficient in the transition region to be computed. Stewartson's [27] transformation is used to relate incompressible and compressible quantities. The method is invalid when the transition region includes separated flow or a shock wave or extends into the wake (see Appendix B for details).

Turbulent Boundary Layer

The turbulent boundary layer and wake is calculated with the lag-entrainment integral method of Green et al. [28] modified by East et al. [29] in either the direct mode with u_i specified or in the inverse mode with the mass flux defect Q specified. Here $Q = \rho_i u_i \delta^*$ where ρ_i is the inviscid density on the airfoil or wake centerline. Both attached and thin separated turbulent flow can be calculated. This method is based on the solution of three ordinary differential equations: the momentum integral equation, entrainment equation and a lag equation derived from the differential turbulent kinetic energy equation. The original integral boundary layer equations of Green et al. [28] were extended to include physical surface transpiration. The extended momentum integral equation is

$$\frac{d\theta}{ds} = \frac{C_f}{2} - (H + 2 - M^2)\frac{\theta}{u_e}\frac{du_e}{ds} + m_w$$

where $m_w = (\rho_w v_w)/(\rho_e u_e)$ is the nondimensional transpiration mass flux. Here the subscripts e and w denote the edge of the boundary layer and airfoil surface, respectively, s is the arclength in the streamwise direction along the airfoil or wake centerline, θ is the momentum thickness, u is the speed, C_f is the skin friction coefficient, H is the shape factor, M is the local Mach number and ρ is the density. The equation for the entrainment coefficient C_E given by Green et al. [28] is extended [1] to

$$C_E = \frac{1}{\rho_e u_e}\frac{d}{ds}\int_o^\delta \rho u dn - m_w$$

ere $C_E = V_E/u_e$, V_E is the entrainment velocity (positive for entrainment) and n is the coordinate normal to the airfoil surface. Using the definition

$$H_1 = \frac{1}{\theta}\int_o^\delta \frac{\rho u}{\rho_e u_e} dn$$

results in the modified entrainment equation [1]

$$\frac{d\bar{H}}{ds} = \frac{d\bar{H}}{dH_1}\{C_E + m_w - H_1\left[\frac{C_f}{2} + m_w - (H+1)\frac{\theta}{u_e}\frac{du_e}{ds}\right]\}/\theta$$

where $\bar{H}$ is Head's shape factor, $\bar{H} = \frac{1}{\theta}\int_0^\delta \frac{\rho}{\rho_e}(1 - \frac{u}{u_e})dn$.

In the method of Green et al. [28] the skin friction coefficient C_f is computed from a correlation depending on the value of the flat-plate (zero pressure gradient) skin friction coefficient C_{fo} corresponding to the momentum thickness Reynolds number Re_θ of the flow. The value of this flat-plate skin friction coefficient is modified to account for the effects of transpiration by using the relation given by Kays and Crawford [30]

$$C_{fo} = C_{fos}\left[\frac{\ell_n(1+B_f)}{B_f}\right]^{1.25}(1 + B_f)^{0.25}$$

ere C_{fos} is the flat-plate (zero pressure gradient) skin friction coefficient for a nonporous surface and $B_f = m_w/(C_{fo}/2)$. The value of C_{fo} is determined by Newton iteration. It is assumed that the other empirical correlations used in the method of Green et al. [28] and modified by East et al. [29] are approximately the same for the case of a transpired boundary layer.

In the inverse mode the dependent variables are u_e, $\bar{H}$ and C_E. The form of the equations is

$$\frac{du_e}{ds} = -\frac{A}{B} + \frac{1}{B}\frac{dQ}{ds}$$

$$\frac{d\bar{H}}{ds} = C + D\frac{du_e}{ds}$$

$$\frac{dC_E}{ds} = E + F\frac{du_e}{ds}$$

The expressions for the coefficients are given in Appendix C. The boundary layer and wake on the upper and lower sides of the airfoil and wake centerline are computed separately. The wake centerline is taken to be a cubic polynomial with the four coefficients determined from the locations and slopes of the trailing edge and the assumed location of the end of the wake centerline. The skin friction coefficient is set equal to zero in the wake. The starting value for u_e is u_i. When transition is enforced the starting value for Q is determined in either of two ways. One way is to assume continuity of Q. The other way is to compute Q by assuming that it has the value that a flat-plate boundary layer would have at the same distance from the leading edge. The starting values for $\bar{H}$ and C_E are found following the method given by Olling [1]. The correction for longitudinal surface curvature suggested by Green et al. [29] was incorporated by Olling [1]. The system of equations is integrated with a 4th-order Runge-Kutta method (Ferziger [31]). The streamwise step size is clustered toward the leading and trailing edges and is smaller than that of the inviscid code. The first derivative of the forcing function is calculated in the supersonic region by first-order accurate upstream differencing and in the subsonic region by the second-order accurate differencing for a nonuniform step size presented as Eq. (3.14.3) of Ferziger [31].

FINITE-DIFFERENCE BOUNDARY-LAYER CODE

The finite-difference compressible boundary layer code presented by Drela [32] was adapted to the present coupling approach. This code can compute compressible laminar, transitional and turbulent flow that is attached or separated. Modifications were made by Olling [1] to the calculation of the inner eddy viscosity for turbulent separated flow. Surface transpiration effects were incorporated. The intermittency factor of Abu-Ghannam and Shaw [26] was used in the transition region. This code is based on a variation of Keller's box scheme [33,34].

The governing equations are the continuity equation, linear momentum equation in the streamwise direction and the total enthalpy equation. The Cebeci-Smith [34] two-layer algebraic eddy viscosity formulas are used. These equations are nondimensionalized, and then transformed variables are introduced which permit the calculation of flow near the stagnation point. The coupled system of equations is discretized on the shifted box grid [32] and Newton iteration is applied to determine the iterates of the unknown variables. This procedure leads to a block tridiagonal system of equations in which the blocks are 3x3 matrices. The eddy viscosity is also linearized during the Newton iteration procedure and this leads to quadratic convergence of the solution for both laminar and turbulent flow.

Four different forcing functions can be used. In the direct mode u_i is specified. In the inverse mode δ^*, Q or C_f can be specified. It was found by numerical experiments that the solution would not converge when Q was specified at the stagnation point.

A modified Reyhner-Flugge-Lotz approximation is applied in the separated flow. This consisted of eliminating the contribution of the convective momentum term to the variable iterates (the terms inside the 3 x 3 blocks) but retaining its contribution to the residues.

The finite-difference code was chosen over a laminar integral boundary-layer code capable of computing laminar separated flow for two reasons. A laminar integral boundary-layer code based on a modified Klineberg-Lees [35] method was developed by Olling [1], but it was found that the code could not be used very near the stagnation point because the integral boundary layer equations possess a singularity there. This would render the method inappropriate if a leading edge separation bubble occurred. Also a laminar integral boundary-layer code cannot compute the transitional region (unless the approximate procedure of LeBalleur [13] is applied) and the empirical method of Abu-Ghannam and Shaw [26] is inapplicable when the transition region contains separation or a shock wave.

Thus, for these special cases, the finite-difference method is most appropriate.

COUPLING BOUNDARY CONDITIONS

Total Transpiration Velocity

The coupling boundary conditions in the inviscid code on the airfoil and wake centerline are a total transpiration velocity v_n normal to the airfoil and jump conditions on the velocity components normal and tangent to the assumed wake centerline. The total transpiration velocity v_n consists of two parts: an equivalent transpiration velocity v_b due to the boundary-layer displacement effect and a physical mass-weighted transpiration velocity v_c due to suction or blowing through the porous airfoil surface, such that

where $$v_n = v_b + v_c$$

$$v_b = \frac{1}{\rho_i}\frac{dQ}{ds} \qquad \text{and} \qquad v_c = \frac{\rho_w}{\rho_i} v_w$$

Here ρ_w and v_w are the density and velocity of the physically transpired fluid, respectively. The sign of v_n is positive for blowing (i.e., a source). It is assumed that ρ_w is equal to the adiabatic wall density

$$\rho_w = \rho_i / \left(1 + r\,\frac{(\gamma-1)}{2} M^2\right)$$

where r is the recovery factor, γ is the specific heat ratio, and M is the local Mach number. For laminar flow, $r = (Pr)^{\frac{1}{2}}$ and for fully turbulent flow $r = (Pr)^{1/3}$, where Pr is the Prandtl number. For sitional flow, it is assumed that $r = (Pr)^{(\frac{1}{2}-\gamma_{tr}/6)}$ where γ_{tr} is the intermittency factor, $0 \le \gamma_{tr} \le 1$, $\gamma_{tr} = 0$ for laminar flow, and $\gamma_{tr} = 1$ for fully turbulent flow. The displacement thickness in the definition of Q is

$$\delta^* = \frac{1}{\rho_{iw} u_{iw}} \int_0^{\delta} (\rho_i u_i - \rho u)\, dn$$

The velocity jumps on the wake centerline are (Lock and Firmin [3])

$$\Delta v_n = \frac{1}{\rho_{iu}}\left(\frac{dQ}{ds}\right)_u + \frac{1}{\rho_{i\ell}}\left(\frac{dQ}{ds}\right)_\ell$$

$$\Delta u_t = -\left[K_u^* \frac{Q_u}{\rho_{iu}}\left(1 + 1/H_u\right) + K_\ell^* \frac{Q_\ell}{\rho_{i\ell}}\left(1 + 1/H_\ell\right)\right]$$

where Δ indicates a jump, the subscripts u, ℓ denote the upper and lower sides of the wake centerline, $H = \delta^*/\theta$ is the shape factor and K^* is the curvature of the displacement thickness surface

$$K^* = \frac{d\beta}{ds}$$

where β is the streamline slope [19] on the displacement thickness surface. A procedure similar to that of Collyer is used to introduce the jumps in the normal and tangential velocity components into the reduced potential at the points on the upper and lower sides of the wake centerline and at the fictitious points on either side of the wake centerline. The detailed procedure is shown by Olling [1].

The semi-inverse coupling method can be summarized as follows:

1) The potential solution is advanced for a certain number of iterations on up to four increasingly refined grids with $v_n = 0$ on the airfoil surface.

2) The boundary layer code was run in the direct mode with u specified from step 1 until separation or a specified point was reached. At that point the boundary layer code was switched to the inverse mode with an initial guess for Q .

3) Wigton's or Carter's formulas for updating the Q values are applied (see Appendix D). The transpiration velocity and jumps in the velocity components along the wake centerline are computed.

4) The potential solution is advanced for one to five iterations on the finest grid being used, with the boundary conditions held constant. During the first nine coupling cycles the relaxation factor was equal to unity. After that the relaxation parameter was equal to 1.7 - 1.8 .

5) The boundary layer code was run in the direct mode on the forward part of the airfoil and in the inverse mode on the rest of the airfoil and wake centerline with the Q values determined from step 3.

6) Steps 3 - 5 are repeated until the error measure $(u_e/u_i - 1)$ is less than a specified value or until a maximum number of interaction cycles has been reached.

RESULTS

Based on the detailed analytic and numerical analysis of Olling [1], a package of computer programs, GSD28, was developed [24]. This software performs automatic computational grid generation, full potential finite area inviscid flow solution [15], integral and finite difference method solution of the complete boundary layer with wake, and automatically iteratively couples the inviscid and the viscous part of the flow field.

The first example is for a cascade of solid Sobieczky [16] airfoils, which are not shock-free. The upstream Mach number is 0.80, the Reynolds number based on the chord is 9.1×10^5, $T_\infty = 288K$, $c = 0.076m$, and the freestream turbulence level is 1%. The upstream angle of attack with respect to the horizontal is 40° and the stagger angle with the horizontal is 27.3°. The gap-to-chord ratio is 1.0 . The computational wake extends 2 chord lengths downstream. Three sets of increasingly refined grids were used. The finest grid had 48 cells on both the upper and lower sides of the airfoil, 32 cells along each side of the wake and 16 C-layers of grid cells in the outward direction (Fig. 1). The inviscid code was run for 10 iterations on the first grid, 10 iterations on the second grid and 5 iterations on the third grid. Viscous-inviscid coupling was then initiated. During the coupling, one viscous sweep was performed for each inviscid sweep. The over-relaxation factor for the inviscid code during the coupling was 1.697.

Transition was enforced on the upper side of the airfoil at 3% of the chord and the boundary layer and wake were computed by the integral method. Natural transition was allowed on the lower side of the airfoil, and the boundary layer was computed by the finite-difference method with the wake computed by the integral method. Transition started at $x/c = 0.2357$ and ended at $x/c = 0.5554$.

Wigton's update method was used for the first 400 coupling cycles in the regions computed by the integral

method. Wigton's method was used because during the initial coupling cycles with Carter's update method with a relaxation factor of 0.1, the boundary layer developed oscillations. Carter's update method, with a relaxation factor of 0.1, was therefore used for the last 240 coupling cycles. At the same time, Carter's update method, with a relaxation factor of 0.1, was successfully used for the regions computed by the finite-difference boundary-layer code. The trailing edge treatment explained by Olling [1] was applied. Mach number field is presented in Figure 2. The airfoil surface pressure coefficient distribution is shown in Figure 3. The coupled and pure inviscid solutions exhibit large differences indicating strong viscous-inviscid interaction. The predicted drag coefficient is $C_D = 0.02458$ and the lift coefficient is $C_L = 0.64293$. The predicted turning angle is 16.92°. The total transpiration velocity is presented in Figure 4. A large value is noted at the trailing edge on the upper side of the airfoil. The displacement thickness is shown in Figure 5. The skin friction coefficient is shown in Figure 6. On the upper side of the airfoil, the flow has shock-induced separation between $x/c = 0.369$ and $x/c = 0.496$ and separates again downstream of $x/c = 0.683$. On the lower side of the airfoil, laminar separation starts at $x/c = 0.163$ and reattachment occurs at $x/c = 0.427$ as a transitional flow with the itermittency factor $\gamma_{tr} = 0.66$. When this example was computed with a freestream turbulence level of 5%, natural transition occurred sooner on the lower side of the airfoil and no separation occurred there.

The second cascade flow example is for both a solid and porous NACA 65-(12)10 cascade. The pressure coefficient was experimentally determined for the solid cascade by Briggs [38]. The upstream Mach number is 0.81, the Reynolds number based on the chord is 9.1×10^5, $T_\infty = 288K$, $c = 0.076m$ and the freestream turbulence level is assumed to be 5%. The upstream angle of attack with respect to the horizontal is 45°, and the stagger angle relative to the horizonal is 28.5°. The gap-to-chord ratio is 1.0. The wake extends 2 chord lengths downstream.

In the porous cascade case, a peaked permeability factor distribution on the upper side of the airfoil was used with $\bar{\sigma}_{max} = 0.10$, $x_1 = 0.20$, $x_2 = 1.0$, and $x_m = 0.3586$.

Transition was enforced at 3% of the chord on the upper side of the airfoil and natural transition was allowed on the lower side. The boundary layer and wake on both sides were computed with the integral method. For the lower side of the solid airfoil, computed transition started at $x/c = 0.085$ and ended at $x/c = 0.244$. For the lower side of the porous airfoil, transition started at $x/c = 0.0925$ and ended at $x/c = 0.262$.

The converged solution Mach number field with a contour interval of 0.02 is presented in Figure 7 for the solid cascade case. The pressure coefficient is shown in Figure 8. For the solid cascade, the computations agree fairly well with the experiment except at the beginning of the shock. For the porous cascade, the shock strength is weaker. The C_p curve on the upper side begins to differ from that of the solid case at the start of the porous region. The computed drag coefficient for the solid cascade is $C_D = 0.03086$ and for the porous cascade is $C_D = 0.02755$, a reduction of 10.7%. The computed lift coefficient for the solid cascade is $C_L = 0.74235$ and for the porous cascade is $C_L = 0.76023$, an increase of 2.41%. The computed static-pressure rise, p_2/p_1, for the solid cascade is 1.2546 while the experimental value was 1.244. The value for the porous case is 1.2622. The computed turning angle for the solid cascade is 19.0° while the experimental value was 20.6°. The value for the porous case is 19.97°. The plenum C_p for the porous airfoil is -0.453 while $C_p^* = -0.406$.

Figure 9 illustrates the equivalent and physical mass-weighted transpiration velocities, v_b/a^* and v_c/a^*, and the permeability factor $\bar{\sigma}$ for the porous cascade. Because the plenum C_p is close to C_p^*, physical blowing occurs in the supersonic region ahead of the shock and physical suction takes place behind the shock. The displacement thickness is shown in Figure 10. The skin friction coefficient is presented in Figure 11. For the solid cascade, shock-induced separation occurs between $x/c = 0.41$ and $x/c = 0.45$, and the flow again separates at $x/c = 0.80$. A smooth transition region on the lower side of the airfoil is computed. For the porous cascade, physical blowing ahead of the shock leads to decrease of C_f to near separation, but the flow remains attached. Physical suction behind the shock causes the C_f to increase. Only a small region of trailing edge separation occurs. The momentum thickness, shape factor and mass flux defect are presented in Figures 12, 13 and 14, respectively.

It should be pointed out that all computations were performed on a medium-size computer, HARRIS 800 II. One sweep of the inviscid code on a typical grid used during the coupling required between 5.35 and 5.87 seconds of CPU time. The integral boundary-layer code computed the entire boundary layer and wake and coupling boundary condition in about 5.4 seconds of CPU time. The finite-difference boundary-layer code required an order of magnitude more time, 62.4 seconds of CPU time to compute the boundary layer on one side of the airfoil only.

Conclusions and Recommendations

On the basis of the results presented, it can be concluded that coupled viscous-inviscid calculations of transonic separated cascade flows, with or without physical transpiration, are feasible with the present method [1,24]. However, the semi-inverse coupling method can require a large number of coupling cycles in difficult cases. Part of the reason for this is the slow convergence rate of the SLOR scheme [36] of the inviscid code on the finest grid being used. More efficient inviscid algorithms (e.g., alternating-direction implicit or approximate factorization schemes) are available that could remedy that aspect of the problem. But even without modifying the inviscid algorithm, some improvement of the global convergence could be achieved by simultaneous calculation of the inviscid and viscous equations in the manner of, for example, Wai and Yoshihara [37] but without their viscous ramp model of shock/boundary-layer interaction. Another advantage of that approach would be the elimination of the necessity of specifying an initial guess for the mass flux defect when separation is encountered. Such calculations were made with a modified version of the GSD28 code [1,24]. The nonlifting NACA 0012 airfoil was tested using this approach, and the results were encouraging.

For separating cascade flow, Wigton's update formulas are best for the initial coupling cycles, after

which Carter's update formula can be used to achieve smoother solutions in the shock region.

The pressure correction theory of Lock and Firmin [3] is inappropriate in the region of strong shock waves. A more sophisticated approach is needed. Boundary-layer displacement effects can be much larger in cascades than for isolated airfoils. The shock wave in cascades will often be in a region of transitional flow unless the freestream turbulence level is high. The present integral boundary-layer code cannot handle this situation and transition must be enforced ahead of or at the shock.

The computations show that passive physical transpiration can lead to a reduced drag coefficient and increased lift coefficient for the permeability factor distributions used in the present work. The shock strength can be diminished and shock-induced separation can be eliminated. If the porosity is too large or the porous region extends too far ahead of the shock, it was observed that the induced blowing ahead of the shock may cause separation there. Actually, the aerodynamic performance of airfoils also can be decreased if the porosity is applied in an ad-hoc manner, just as the incorrectly applied "shaving-off" procedure [16] can make shocked airfoils have even stronger shocks.

Consequently, it would be highly desirable to approach the entire concept of porous airfoil design as an inverse problem. Thus, the optimal porosity distribution and its extent should be found so that it corresponds to a minimal possible total aerodynamic drag for the particular airfoil and given global aerodynamic parameters.

APPENDIX A: LAMINAR BOUNDARY LAYER

Rott and Crabtree's [25] compressible Thwaites method for laminar boundary layers is modified as shown below.

From Stewartson's [27] transformation, we have the following relationships between incompressible (subscript I) and compressible quantitites

$$ds_I = C \frac{a_e}{a_\infty} \frac{p_e}{p_\infty} ds \tag{A.1}$$

$$dn_I = \frac{a_e}{a_\infty} \frac{\rho}{\rho_\infty} dn \tag{A.2}$$

$$u_I = \frac{a_\infty}{a_e} u \tag{A.3}$$

$$\frac{du_I}{ds_I} = C^{-1} \frac{a_\infty^2}{a_e^2} \frac{p_\infty}{p_e} \frac{T_o}{T_e} \frac{du}{ds} \tag{A.4}$$

$$\theta_I = \frac{p_e}{p_\infty} \frac{a_\infty}{a_e} \theta \tag{A.5}$$

$$C = \frac{\mu}{\mu_\infty} \frac{T_\infty}{T} \tag{A.6}$$

Here, n is the coordinate normal to the airfoil, and the subscripts ∞ and o denote upstream infinity and stagnation conditions, respectively. The value of θ is computed from

$$\theta = \left| 0.45 \, \nu_o \left(\frac{p_\infty}{p_e}\right)^2 \left(\frac{a_e}{a_\infty}\right)^8 u^{-6} \int_o^s u^5 C \left(\frac{a_\infty}{a_e}\right)^4 \frac{p_e}{p_\infty} \, ds \right|^{1/2} \tag{A.7}$$

where ν_o is the stagnation kinematic viscosity coefficient. The incompressible pressure gradient parameter ℓ_I is

$$\ell_I = \frac{du_I}{ds_I} \frac{\theta_I^2}{\nu_o} = \frac{1}{C} \left(\frac{a_\infty}{a_e}\right)^4 \frac{p_e}{p_\infty} \frac{T_o}{T_e} \frac{\theta^2}{\nu_o} \frac{du}{ds} \tag{A.8}$$

The incompressible shape parameter H_I is computed from ℓ_I using the curve fits to Thwaites' tabulated values presented by Cebeci and Bradshaw [33]

$$\text{for } \ell_I \geq 0 \quad H_I = 2.61 + \ell_I(-3.75 + 5.34\, \ell_I)$$

$$\text{for } \ell_I < 0 \quad H_I = 0.0731/(0.14 + \ell_I) + 2.088 \tag{A.9}$$

The skin friction coefficient is computed from

$$C_f = 2CP \left(\frac{a_e}{a_\infty}\right)^2 M_\infty / (MRe_{\delta_I^*}) \tag{A.10}$$

$$Re_{\delta_I^*} = \frac{u_{I\infty} \delta_I^*}{\nu_{I\infty}} \tag{A.11}$$

$$\delta_I^* = \theta_I H_I \tag{A.12}$$

$$P = \frac{\delta_I^*}{u_I} \left(\frac{\partial u_I}{\partial n_I}\right)_{n_I=0} \tag{A.13}$$

Klineberg and Lees [35] present P and H_I as functions of a parameter "a" for Falkner-Skan velocity profiles. Using a polynomial least squares fit, the following relation was determined for attached flows

$$a = 8.036555z + 41.54676z^2 - 167.6696z^3 + 300.770z^4 + 1546.605z^5 \tag{A.14}$$

where $z = H_I - 0.24711$. Then P was determined from the relation given by Klineberg and Lees [35]. The shape factor is computed from

$$H = H_I \frac{T_o}{T_e} + Pr^{1/2} \left(\frac{T_o}{T_e} - 1\right) \tag{A.15}$$

The displacement thickness is $\delta^* = H\theta$ and the mass flux defect is $Q = \rho_e u_e \delta^*$.

APPENDIX B: TRANSITION REGION

The empirical method of Abu-Ghannam and Shaw [26] for calculating transitional boundary layers is modified for compressibility as shown below. By using Stewartson's [27] transformation, the following relations between incompressible (subscript I) and compressible quantities are found (in addition to Eqs. (A.1), (A.3-A.6))

$$R_{\theta_I} = \frac{\theta_I u_I}{\nu_I} = \frac{P_e}{P_\infty}\left(\frac{a_\infty}{a_e}\right)^2 \frac{\theta u}{\nu_I} \qquad (B.1)$$

$$\lambda_I = \frac{\theta_I^2}{\nu_I}\frac{du_I}{ds_I} = \frac{1}{C}\left(\frac{a_\infty}{a_e}\right)^4 \frac{P_e}{P_\infty}\frac{T_o}{T_e}\frac{\theta^2}{\nu_I}\frac{du}{ds} \qquad (B.2)$$

where the subscript ∞ denotes upstream infinity. The value of ν_I is calculated by finding u_I and from this determining the isentropic temperature and density

$$T_I = T_o\left(1 - \frac{\gamma-1}{2}\left(\frac{u_I}{a_o}\right)^2\right) \qquad (B.3)$$

$$\rho_I = p_o\left(1 - \frac{\gamma-1}{2}\left(\frac{u_I}{a_o}\right)^2\right)^{\frac{\gamma}{\gamma-1}}/(RT_I) \qquad (B.4)$$

and then using Sutherland's equation

$$\nu_I = \mu_I/\rho_I = [1.458\times10^{-6}\ T_I^{1.5}/(T_I+110.4)]/\rho_I \qquad (B.5)$$

The quantities p_o, T_o, a_o are the stagnation pressure, temperature and speed of sound, respectively. The incompressible arc length is found by integrating Eq. (A.1).

The start of transition (subscript S) is determined from the relation

$$(R_\theta)_I \geq (R_\theta)_{IS} \qquad (B.6)$$

where $(R_\theta)_{IS}$ is defined by Eqs. (11)-(13) of Abu-Ghannam and Shaw [26].

The end of transition (subscript E) is determined from finding when

$$s_I \geq s_{IE} \qquad (B.7)$$

where

$$s_{IE} = R_{XIE}\,\nu_{IS}/u_{IS} \qquad (B.8)$$

$$R_{XIE} = R_{XIS} + 16.8(R_{XIS})^{0.8} \qquad (B.9)$$

$$R_{XIS} = s_{IS}\,u_{IS}/\nu_{IS} \qquad (B.10)$$

The momentum thickness at the end of transition depends on the value of

$$C_2 = B^2 - 4A\bar{C} \qquad (B.11)$$

where

$$A = 183.5\ C_1(1.4)\left(\frac{du_I}{ds_I}\right)_E/\nu_{IE} \qquad (B.12)$$

$$B = u_{IE}/\nu_{IE} \qquad (B.13)$$

$$\bar{C} = -540 - 183.5C_1 \qquad (B.14)$$

$$C_1 = R_{IL}\ 10^{-5} - 1.5 \qquad (B.15)$$

$$R_{IL} = (s_{IE} - s_{IS})u_{IS}/\nu_{IS} \qquad (B.16)$$

If $C_2 > 0$, then

$$\theta_{IE} = [-B + (C_2)^{\frac{1}{2}}]/(2A) \qquad (B.17)$$

If $C_2 < 0$, then

$$\theta_{IE} = 0.0368(R_{IL}^{0.8})/B \qquad (B.18)$$

The value of θ_E is found from Eq. (A.5). This value is used to compute H_E and C_{fE} according to the second method suggested in section A.4 of Green et al. [45].

The values of θ, H and C_f in the transition region are found using Eqs. (24), (26) and (32) of Abu-Ghannam and Shaw [26].

APPENDIX C: TURBULENT BOUNDARY LAYER

The coefficients used in Eqs. (4.4)-(4.6) are presented below.

$$A = -\rho_e u_e F_1$$

$$F_1 = H\left(\frac{C_f}{2} + m_w\right) + (1+0.2rM^2)\left[C_E + m_w - H_1\left(\frac{C_f}{2} + m_w\right)\right]\frac{d\bar{H}}{d\bar{H}_1}$$

$$B = [(1-M^2)Q + \rho_e u_e F_2\theta]/u_e$$

$$F_2 = -H(H + 2 - M^2) + (1 + 0.2\ rM^2)(H+1)H_1\frac{d\bar{H}}{d\bar{H}_1} + 0.4rM^2(1 + 0.2M^2)(\bar{H} + 1)$$

$$C = \frac{d\bar{H}}{dH_1}\left\{C_E + m_w - H_1\left(\frac{C_f}{2} + m_w\right)\right\}/\theta$$

$$D = \frac{d\bar{H}}{dH_1}\,H_1(H+1)/u_e$$

$$E = \bar{F}\{2.8[(C_\tau)^{\frac{1}{2}}_{EQ_0} - \lambda(C_\tau)^{\frac{1}{2}}]/(H + H_1) + \left(\frac{\theta}{u_e}\frac{du_e}{dS}\right)_{EQ}\}/\theta$$

$$F = -\bar{F}[1 + 0.075M^2(1 + 0.2M^2)/(1 + 0.1M^2)]/u_e$$

where

$$\bar{F} = (0.02C_E + C_E^2 + 0.8\ C_{f_0}/3)/(0.01 + C_E)$$

$$C_\tau = \tau/(\rho_e u_e^2)$$

τ is the maximum shear stress, r is the recovery factor, the subscripts EQ and 0 denote equilibrium flow and flat-plate flow, respectively, and λ is a scaling factor for effects due to longitudinal streamline curvature and flow convergence or divergence.

The following changes are made to equilibrium quantities:

$$(C_E)_{EQ_0} = H_1\left[\frac{C_f}{2} + m_w - (H+1)\left(\frac{\theta}{u_e}\frac{du_e}{ds}\right)_{EQ_0}\right] - m_w$$

$$\left(\frac{\theta}{u_e}\frac{du_e}{ds}\right)_{EQ} = \left\{\frac{C_f}{2} + m_w - [(C_E)_{EQ} + m_w]/H_1\right\}/(H+1)$$

APPENDIX D

Wigton's [14] formulas for updating the Q values between each interaction cycle are as follows:

for $M < 1$

$$Q^{n+1} = Q^n + \frac{\omega_1 \bar{\beta}\rho_i \, Bu_i}{\nu B - \bar{\beta}\rho_i}\left(\frac{u_e}{u_i} - 1\right)$$

for $M > 1$

$$Q^{n+1} = Q^n + \frac{\omega_2 B \bar{\beta}\rho_i}{(\nu B)^2 + (\bar{\beta}\rho_i)^2}\left[B\left(\frac{du_e}{ds} - \frac{du_i}{ds}\right) - \bar{\beta}\rho_i\left(\frac{u_e}{u_i} - 1\right)\right]$$

where M is the local Mach number, $\nu = \pi/\Delta s$, δs is the step size, $\bar{\beta} = |1 - M^2|^{\frac{1}{2}}$, B is the coefficient in the momentum integral equation written in the form

$$\frac{dQ}{ds} = A + B\frac{du_e}{ds}$$

and ω_1 and ω_2 are relaxation factors (equal to unity in Wigton's analysis).

Carter's [12] update formula is

$$Q^{n+1} = Q^n\left[1 + \omega\left\{\frac{u_e}{u_i} - 1\right\}\right]$$

where ω is a relaxation factor.

REFERENCES

1. Olling, C. R., "Viscous-Inviscid Interaction in Transonic Separated Flow Over Solid and Porous Airfoils and Cascades," Ph.D. Dissertation, Department of Aerospace Eng. and Eng. Mechanics, The Univ. of Texas as Austin, Dec. 1985.

2. Lock, R. C., "A Review of Methods for Predicting Viscous Effects on Airfoils and Wings at Transonic Speeds," Proceedings AGARD Conf. on Comput. of Viscous-Inviscid Interations, 1980, AGARD CP 291, 1981, Paper 2.

3. Lock, R. C. and Firmin, M. C. P., "Survey of Techniques for Estimating Viscous Effects in External Aerodynamics, in P. L. Roe (ed.), Proceedings of the IMA Conference on Numerical Methods in Aero. Fluid Dynamics, Reading, 1980. New York: Academic Press, 1982, pp. 337-430.

4. Melnik, R. E., "Turbulent Interaction on Airfoils at Transonic Speeds -- Recent Developments," Proc. AGARD Conf. on Comput. of Viscous-Inviscid Interactions, 1980, AGARD CP 291, Paper 10.

5. LeBalleur, J. C., "Calcul de Ecoulments a Forte Interaction Visqueee au Moyen de Methodes de Couplage," Proc. AGARD Conf. on Comput. of Viscous-Inviscid Interactions, 1980, AGARD CP 291, Paper 1.

6. Jameson, A., "The Evolution of Computational Methods in Aerodynamics," J. Appl. Mech., Vol. 50, 1983, pp. 1052-1070.

7. Cebeci, T., Stewartson, K. and Whitelaw, J. H., "Calculation of Two-Dimensional Flow Past Airfoils, in Numerical and Physical Aspects of Aerodynamic Flows, II. New York: Springer-Verlag, 1984, pp. 1-40.

8. Drela, M. and Thompkins, Jr., W. T., "A Study of Non-Unique Solutions of the Two-Dimensional Boundary Layer Equations at Laminar Separation and Reattachment Points," in Second Symposium on Numerical and Physical Aspects of Aerodynamic Flows, 17-20 January 1983, California State Univ., Long Beach, 1983.

9. Hirsch, C. and Janssens, P., "Viscous-Inviscid Interactions in Cascades," Israel J. Technol., Vol. 20, 1982, pp. 109-126.

10. Dvorak, F. A. and Choi, D. H., "Separation Model for Two-Dimensional Airfoils in Transonic Flow," AIAA J., Vol. 22, 1984, pp. 1064-1070.

11. Murman, E.M. and Bussing, T.R.A., "On the Coupling of Boundary- Layer and Euler Equation Solutions," in Numerical and Physical Aspects of Aerodynamic Flows II. New York: Springer-Verlag, 1984, pp. 313-326.

12. Carter, J.E., "A New Boundary Layer Inviscid Interaction Technique for Separated Flow," Proc. AIAA 4th Comp. FLuid Dyn. Conf., 1979, pp. 45-55.

13. LeBalleur, J.C. "Strong Matching Method for Computing Transonic Viscous Flows Including Wakes and Separations Lifting Airfoils." La Recherche Aerospatiale (English edition), No. 1981-3, 1981, pp. 21-45.

14. Wigton, L.B., "Viscous-Inviscid Interaction in Transonic Flow." Ph.D. Thesis, Univ. of California, Berkeley, 1981.

15. Gordon, R. and Rom, J. "Transonic Viscous/Inviscid Interaction Over Airfoils for Separated Laminar or Turbulent Flows," AIAA J., Vol. 19, 1981, pp. 545-552.

16. Dulikravich, G. S. and Sobieczky, H., "Shockless Design and Analysis of Transonic Cascade Shapes," AIAA J., Vol. 20, 1982, pp. 1572-1578.

17. Savu, G. and Trifu, O., "Porous Airfoils in Transonic Flow," AIAA J., Vol. 22, 1984, pp. 989-991.

18. Savu, G., Trifu, O. and Dumitrescu, L. Z., "Suppression of Shocks on Transonic Airfoils," 14th Int'l. Symp. on Shock Tubes and Waves, Sydney, 1983.

19. Thiede, P., Krogmann, P. and Stanewsky, E., "Active and Passive Shock/Boundary-Layer Interaction Control on Supercritical Airfoils," in Improvement of Aerodynamic Performance Through Boundary Layer Control and High Lift Systems, AGARD CP-365, 1984, Paper 24.

20. Krogmann, P., Stanewsky, E. and Thiede, P., "Effects of Suction on Shock/Boundary-Layer Interaction and Shock-Induced Separation," J. Aircraft, Vol. 22, 1985, pp. 37-42.

21. Nagamatsu, H. T., Ficarra, R. V. and Dyer, R., "Supercritical Airfoil Drag Reduction by Passive Shock Wave/Boundary Layer Control in the Mach Number Range .75 to .90," AIAA 23rd Aerospace Sciences Meeting, Jan. 14-17, 1985, Reno, Nevada, AIAA Paper 85-0207, 1985.

22. Ram, R. B., Vemuru, C. S. and Harvey, W. D., "Hybrid Approach to Steady Transonic Normal Shock-Compressible Laminar Boundary Layer Interactions Over Airfoils with Suction," AIAA Paper 85-0522, AIAA Shear Flow Control Conference, March 12-14, 1985, Boulder, CO.

23. Chen, C. -L., Chow, C. -Y., Holst, T. L. and Van Dalsem, W. R., "Numerical Study of Porous Airfoils in Transonic Flow," NASA TM 86713, May 1985.

24. Dulikravich, G. S. and Olling, C. R., "GSD28-Fortran Program for Analysis and Design of Shock-Free Transonic Airfoils and Turbomachinery Cascades Including Viscous/Inviscid Interaction," Computational Fluid Dynamics Group Research Report 100-85, Dept. of Aero. Eng. and Eng. Mech., The Univ. of Texas at Austin, September 1985.

25. Rott, N. and Crabtree, L. F., "Simplified Laminar Boundary-Layer Calculations for Bodies of Revolution and for Yawed Wings," J. Aero. Sci., Vol. 19, 1952, pp. 553-565.

26. Abu-Ghannam, B. J. and Shaw, R., "Natural Transition of Boundary Layers -- The Effects of Turbulence, Pressure Gradient, and Flow History," J. Mech. Eng. Sci., Vol. 22, 1980, pp. 213-228.

27. Stewartson, K., "Correlated Incompressible and Compressible Boundary Layers," Proc. Roy. Soc. (London), Ser. A., Vol. 200, 1949, pp. 213-228.

28. Green, J. E., Weeks, D. J. and Brooman, J. W. F., "Prediction of Turbulent Boundary Layers and Wakes in Compressible Flow by a Lag-Entrainment Method," Aero. Res. Coun., Reports and Memoranda 3791, 1973.

29. East, L. F., Smith, P. D. and Merryman, P. J., "Prediction of the Development of Separated Turbulent Boundary Layers by the Lag-Entrainment Method." R.A.E. TR-77046, 1977.

30. Kays, W. M. and Crawford, M. E., Convective Heat and Mass Transfer, 2nd. Ed. New York: McGraw-Hill, 1980.

31. Ferziger, J. H., Numerical Methods for Engineering Application. New York: John Wiley & Sons, 1981.

32. Drela, M., "A New Transformation and Integration Scheme for the Compressible Boundary Layer Equations, and Solution Behavior at Separation," M.I.T. Gas Turbine and Plasma Dynamics Laboratory, GTL Report 172, 1983.

33. Cebeci, T. and Bradshaw, P., Momentum Transfer in Boundary Layers. Washington, D.C.: Hemisphere Publishing Corp., 1977.

34. Bradshaw, P., Cebeci, T. and Whitelaw, J. H., Engineering Calculation Methods for Turbulent Flow. New York: Academic Press, 1981.

35. Klineberg, J. M. and Lees, L., "Theory of Laminar Viscous-Inviscid Interactions in Supersonic Flow," AIAA J., Vol. 7, 1969, pp. 2211-2221.

36. Olling, C. R. and Dulikravich, G. S., "Transonic Cascade Flow Analysis Using Viscous/Inviscid Coupling Concepts," AIAA Paper 84-2159, AIAA 2nd Applied Aerodynamics Conf., August 21-23, 1984, Seattle WA.

37. Wai, J. C. and Yoshihara, H., "Viscous Transonic Flow Over Airfoils," in Seventh Int'l. Conf. on Numer. Meth. in Fluid Dynamics. New York: Springer-Verlag, 1981, pp. 417-411.

38. Briggs, W. B., "Effect of Mach Number on the Flow and Application of Compressibility Corrections in a Two-Dimensional Subsonic-Transonic Compressor Cascade Having Varied Porous-Wall Suction at the Blade Tips." NACA TN 2649, 1952.

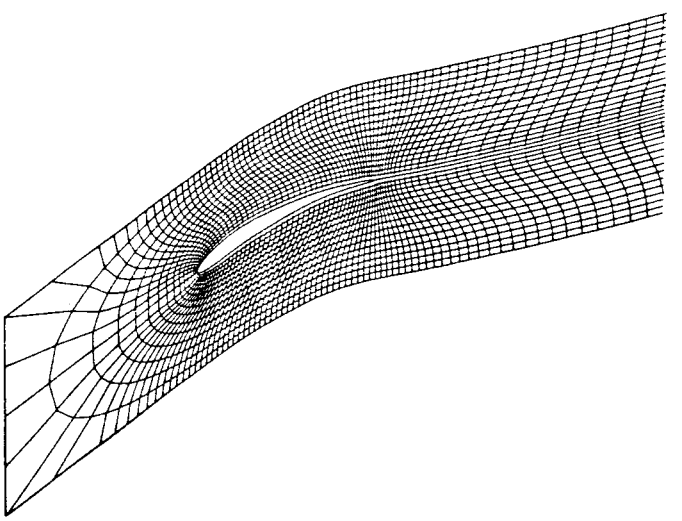

Figure 1 Computational Grid, Sobieczky Cascade

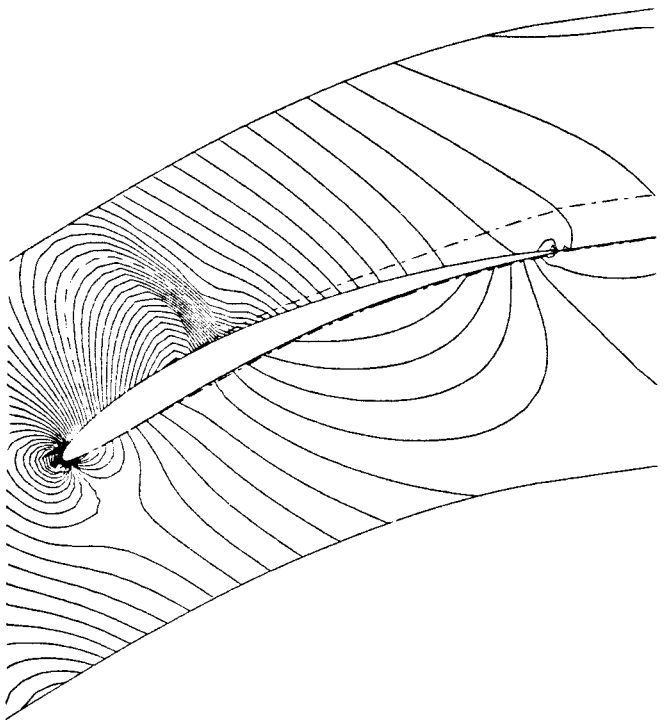

Figure 2 Mach Number Field, Solid Sobieczky Cascade

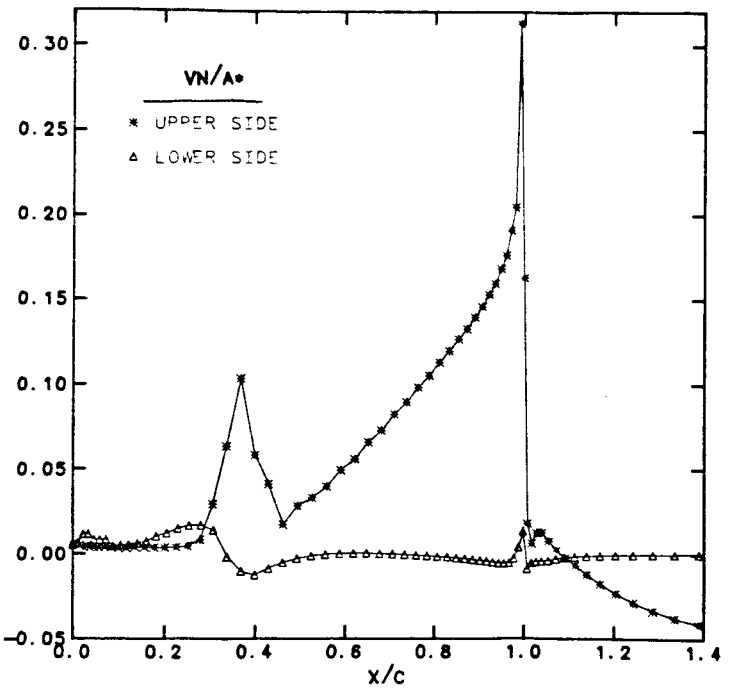

Figure 4 Total Transpiration Velocity, v_n/a^*, Solid Sobieczky Cascade

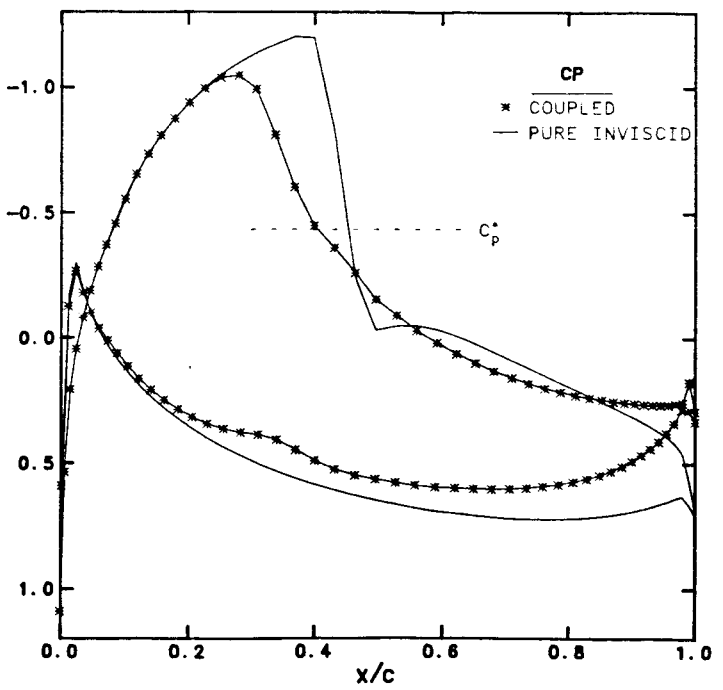

Figure 3 Pressure Coefficient Distribution, C_p, Solid Sobieczky Cascade

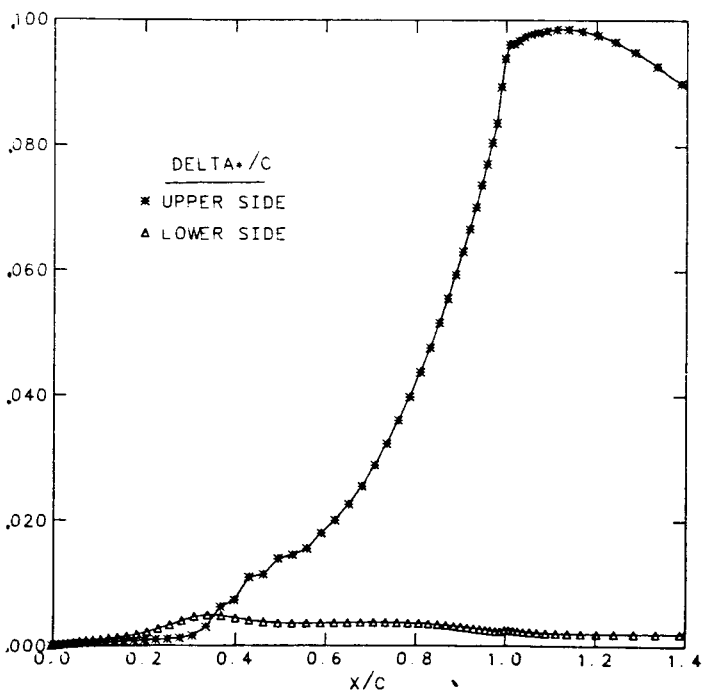

Figure 5 Displacement Thickness, δ^*/c, Solid Sobieczky Cascade

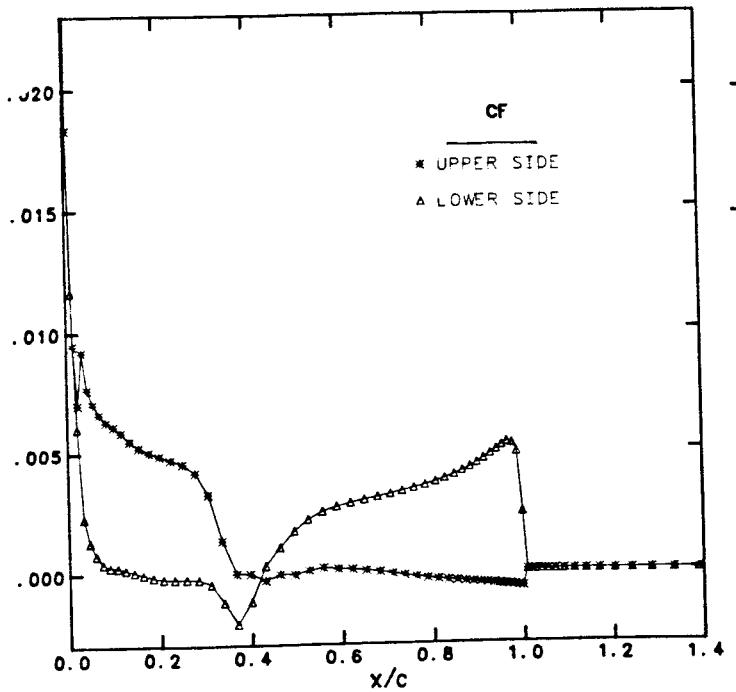

Figure 6 Skin Friction Coefficient, C_f, Solid Sobieczky Cascade

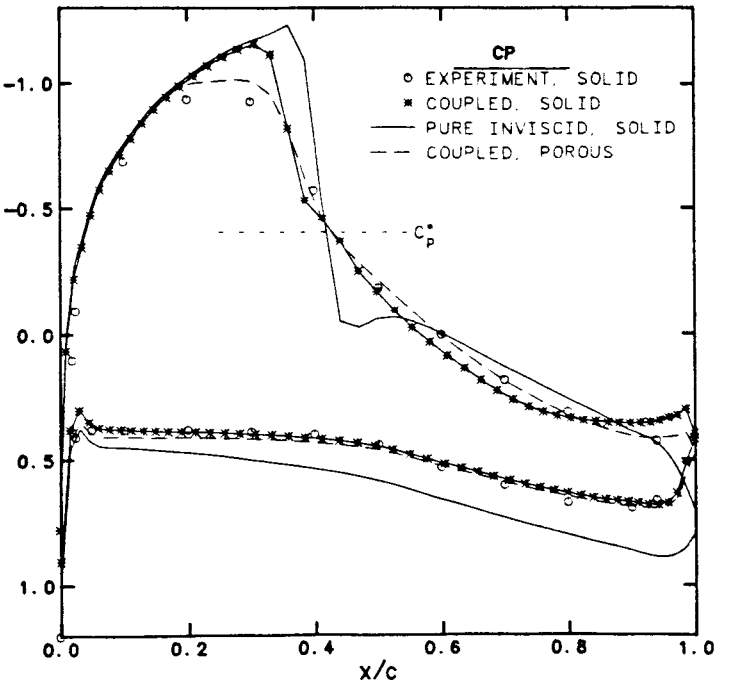

Figure 8 Pressure Coefficient Distribution, C_p, Solid and Porous NACA 65-(12)10 Cascades

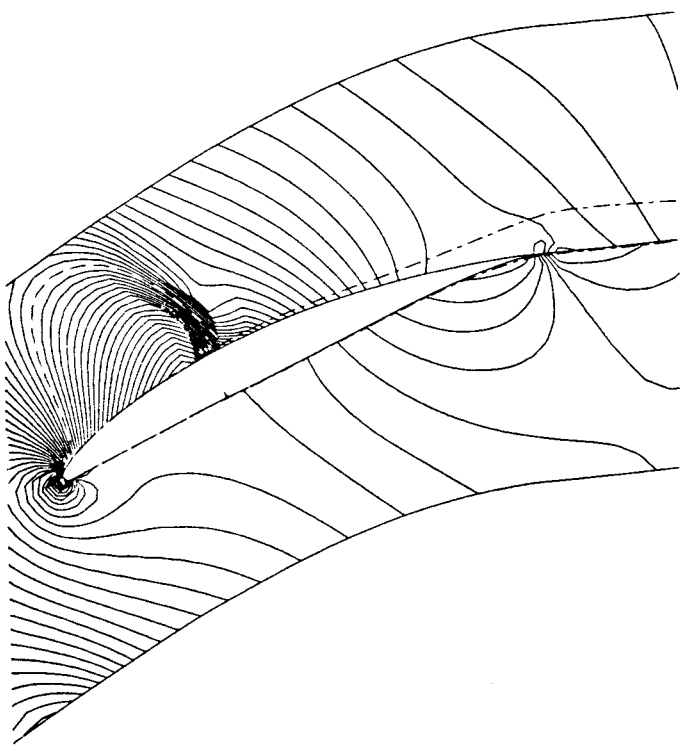

Figure 7 Mach Number Field Solid NACA 65-(12)10 Cascade

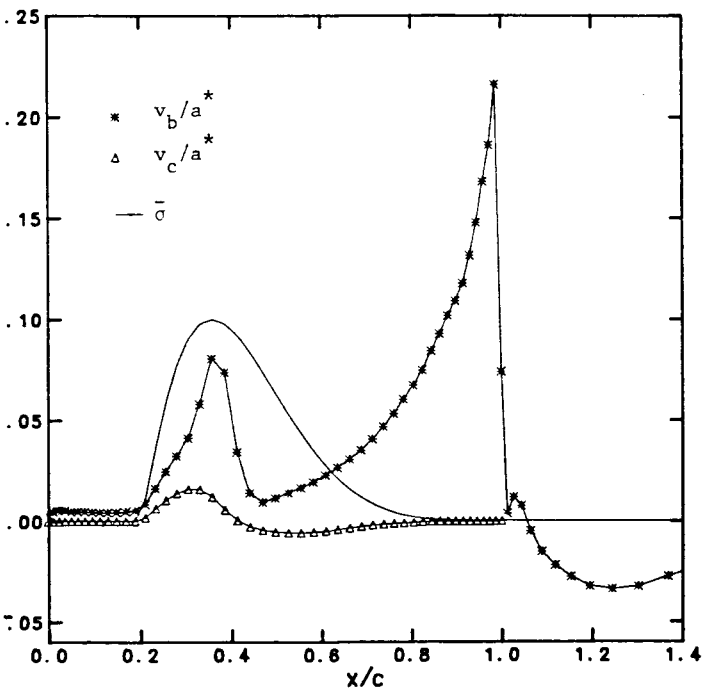

Figure 9 Equivalent and Physical Mass-Weighted Transpiration Velocities, v_b/a^* and v_c/a^*, and the Permeability Factor $\bar{\sigma}$, Upper Side of Porous NACA 65-(12)10 Cascade

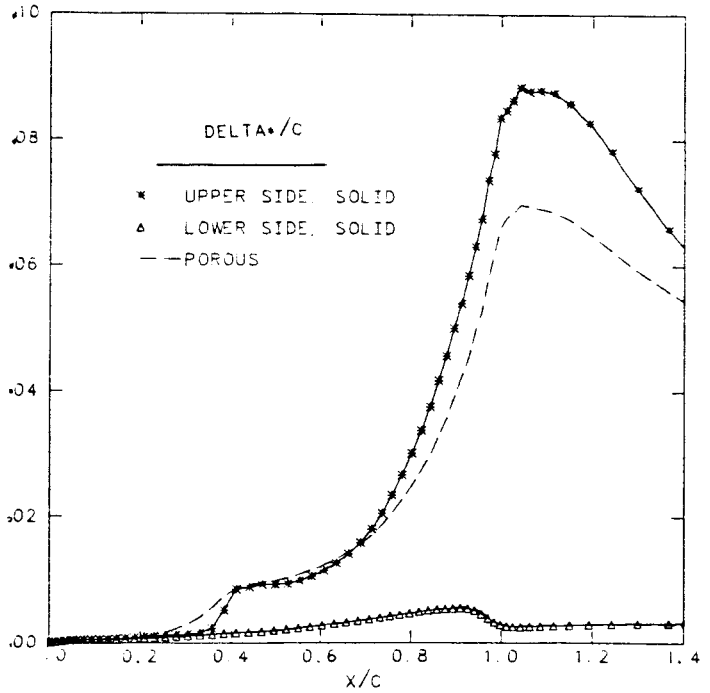

Figure 10 Displacement Thickness, δ^*/c , Solid and Porous NACA 65-(12)10 Cascades

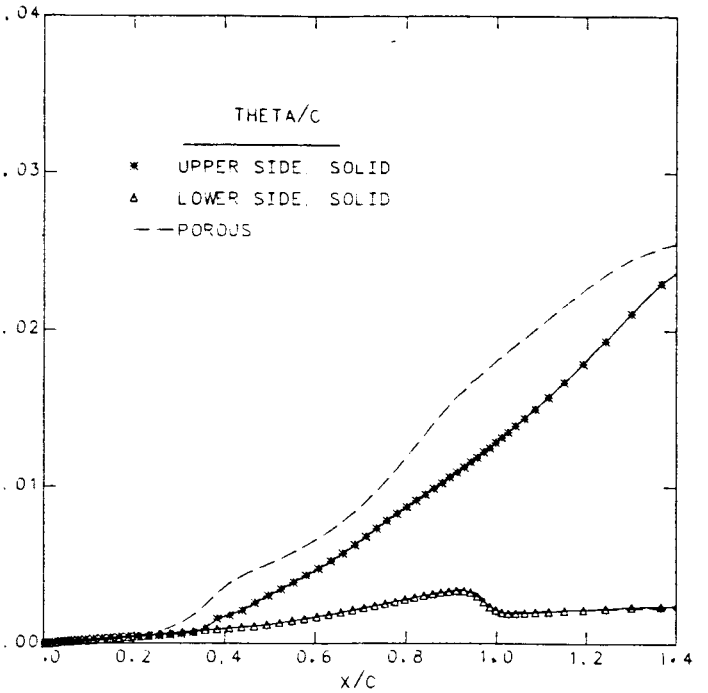

Figure 12 Momentum Thickness, θ/c , Solid and Porous NACA 65-(12)10 Cascades

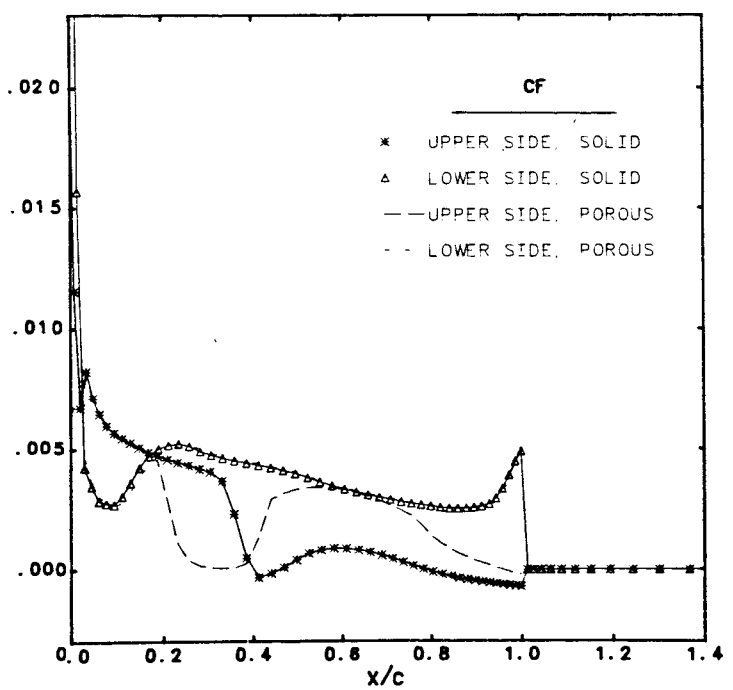

Figure 11 Skin Friction Coefficient, C_f , Solid and Porous NACA 65-(12)10 Cascades

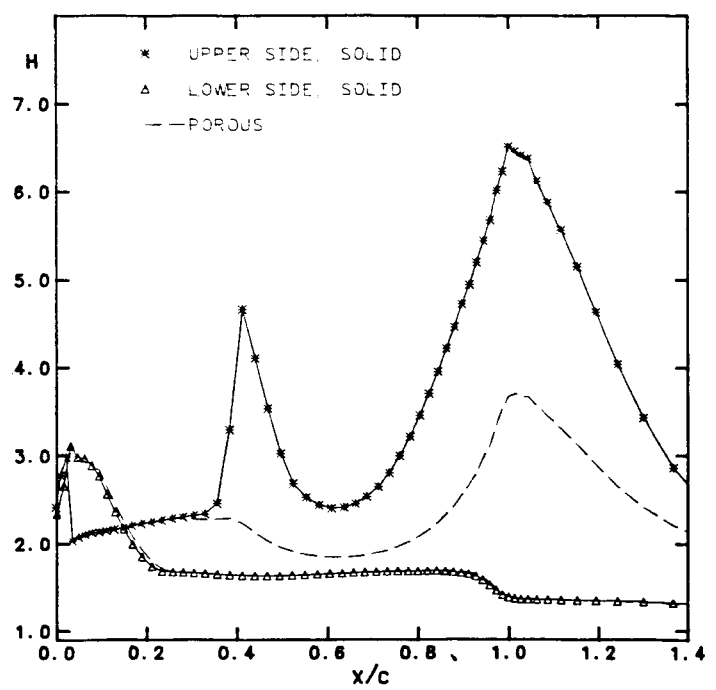

Figure 13 Shape Factor, H , Solid and Porous NACA 65-(12)10 Cascades

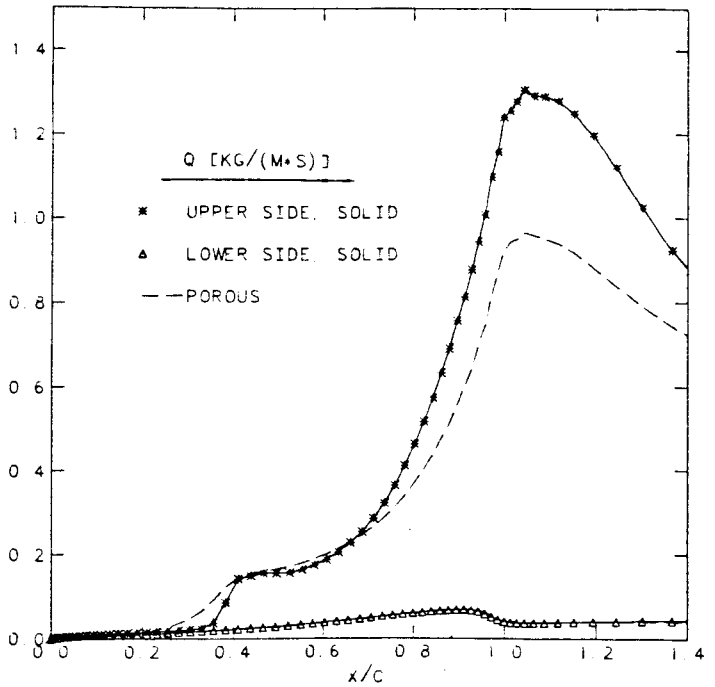

Figure 14 Mass Flux Defect, Q , Solid and Porous NACA 65-(12)10 Cascades